


Article

Durability of Ternary Cements Based on New Supplementary Cementitious Materials from Industrial Waste

Isabel Fuencisla Sáez del Bosque ¹, María Isabel Sánchez de Rojas ^{2,3} , Gabriel Medina ⁴, Sara Barcala ³ and César Medina ^{1,3,*} 

- ¹ Department of Construction, School of Engineering, Institute for Sustainable Regional Development (INTERRA), University of Extremadura, 10003 Cáceres, Spain; isaezdelu@unex.es
- ² Departamento de Cementos y Reciclado de Materiales, Instituto de Ciencias de la Construcción Eduardo Torroja (IETcc-CSIC), c/Serrano Galvache, 28033 Madrid, Spain; srojas@ietcc.csic.es
- ³ Sostenibilidad en Materiales de Construcción, Universidad de Extremadura, Unidad Asociada al CSIC, 10003 Cáceres, Spain; cemedmart@yahoo.es
- ⁴ Departamento Ingenierías Mecánica, Informática y Aeroespacial, Escuela de Ingenierías Industrial e Informática, Universidad de León, Campus de Vegazana, s/n, 24071 León, Spain; gmedinaia@gmail.com
- * Correspondence: cmedinam@unex.es

Abstract: Cement-based materials decay with exposure to aggressive agents, a development that raises infrastructure operation and maintenance costs substantially. This paper analyses the inclusion of ultrafine construction and demolition ($U_{C\&DW}$) and biomass-fuelled power plant (BA) waste as pozzolanic additions to cement in pursuit of more sustainable and eco-respectful binders and assesses the durability of the end materials when exposed to seawater, chlorides (0.5 M NaCl) or sulphates (0.3 M Na_2SO_4). The effect of adding silica fume (SF) at a replacement ratio of 5% was also analysed. Durability was determined using the methodology proposed by Koch and Steinegger, whilst microstructural changes were monitored with mercury intrusion porosimetry (MIP), X-ray diffraction (XRD) and scanning electron microscopy (SEM) for a fuller understanding of decay processes. According to the findings, the new blended cements containing 20% $U_{C\&DW}$ + 10%BA or 20% $U_{C\&DW}$ + 20%BA + 5%SF resist the attack by the aggressive media studied, with a 56-d corrosion index of over 0.7. The composition of the reaction products generated with the attack is essentially the same in OPC and the SCM-bearing materials. The results show that the optimal replacement ratio for SCM is 30%.

Keywords: biomass ash; construction and demolition waste; supplementary cementitious materials; corrosion index; cement pastes; durability



Citation: Sáez del Bosque, I.F.; Sánchez de Rojas, M.I.; Medina, G.; Barcala, S.; Medina, C. Durability of Ternary Cements Based on New Supplementary Cementitious Materials from Industrial Waste. *Appl. Sci.* **2021**, *11*, 5977. <https://doi.org/10.3390/app11135977>

Academic Editor: Doo-Yeol Yoo

Received: 1 June 2021

Accepted: 25 June 2021

Published: 27 June 2021

Publisher's Note: MDPI stays neutral with regard to jurisdictional claims in published maps and institutional affiliations.



Copyright: © 2021 by the authors. Licensee MDPI, Basel, Switzerland. This article is an open access article distributed under the terms and conditions of the Creative Commons Attribution (CC BY) license (<https://creativecommons.org/licenses/by/4.0/>).

1. Introduction

The physical, chemical, mechanical and biological actions affecting concrete structures throughout their service life compromises their durability and compliance with the ultimate limit state and service standards to which they were designed. The result is substantial yearly repair and maintenance costs, which in 2016 came to $\sim \$123 \times 10^9$ worldwide according to ASCE 2017 data on infrastructures [1]. Islam et al. [2], in turn, reported that maintenance costs amount to 14% to 20% of design costs in the UK, Hong Kong and Australia.

The presence of physical-chemical pathological processes in such structures is associated with parameters (choice of materials, type of environmental exposure, w/c ratio in concrete, structural shapes, etc.) defined in project stages ranging from design and construction to operation [3]. When choosing materials, the type of binder (cement), as the concrete component that interacts most readily with aggressive media (sulphates, chlorides, seawater, etc.) in the environment is of particular relevance to durability. Such interaction directly and indirectly induces the formation of expansive products that prompt cracking

and/or surface spalling to the detriment of the bearing section of the concrete. Given that cement susceptibility to such action depends on the chemical composition, crystalline or gelatinous nature and porosity of cement hydration products, those factors play a decisive role in the reactions with aggressive agents. The presence of calcium silicate or aluminate hydrates and especially portlandite is therefore a determinant in cement durability [4].

Along those lines, blending supplementary cementitious materials (SCMs) into cement or concrete is known to improve concrete structure durability [5]. Pozzolanic SCMs in particular favour durability due to their effect on pore system refinement and reduction of pore solution alkalinity and portlandite content in cement matrices [4,6]. In addition to those technical advantages, the use of SCMs carries social and environmental benefits associated with lower natural resource consumption and the valorisation of industrial by-products, as well as a significant decline in CO₂ emissions. CEM II/A-LL or L manufacture generates 16.2% and CEM III/B manufacture 73.0% less of that greenhouse gas than CEM I [7].

Against that backdrop, the scientific community has shown a growing interest in the last 10 years in identifying SCMs that may serve as alternatives to the silica fume, fly ash, blast furnace slag, natural or calcined pozzolans and limestone envisaged in European standard EN 197-1 [8]. One of the most prominent lines of research underway involves the assessment of the mechanical viability of new SCMs sourced from construction and demolition (C&DW) and agroforestry waste in the formulation of more sustainable binary eco-cements.

In 2016, the European Union alone generated 923.9 Mt of C&DW, accounting for around 35% of all the solid waste produced by its 28 members [9]. Those by-products can be separated, crushed and sieved to yield recycled aggregate (RA), in turn classified under three categories depending on concrete (Rc) and masonry (Rb) content [10]: concrete RA (Rc \geq 90%; Rb \leq 10%), mixed RA (Rc < 90%; Rb \leq 30%) and mixed masonry RA (Rc < 70%; Rb > 30%). Whilst the coarse (>4 mm), and especially the concrete, fraction have been extensively researched [11,12] for use as the granular skeleton in recycled concrete, little scientific–technical knowledge has been collected on the fine (<4 mm) and ultrafine (<0.125 μ m) fractions. The valorisation of those materials, comprising 30% to 40% of all C&DW [13], is a challenge to be confronted if circular economy principles are to be instituted in the construction industry.

The use of C&DW ultrafines as SCMs in new cements is an innovative line of work undertaken in recent years by a number of authors, whose interest has focused primarily on the mechanical performance of pastes and/or mortars bearing those materials as partial (3% to 30%) cement replacements. The consensus conclusion reached [14–18] is that GRC contains SiO₂, Al₂O₃ and Fe₂O₃ ($44\% \leq \text{SiO}_2 + \text{Al}_2\text{O}_3 + \text{Fe}_2\text{O}_3 \leq 59\%$), along with CaO (42% to 16%) and exhibits low pozzolanicity and hydraulicity. Its filler effect likewise-identified would favour hydration, providing nucleation sites that would densify the cement matrix microstructure. Masonry and mixed C&DW ultrafines [19–22] comprise essentially SiO₂, Al₂O₃ and Fe₂O₃ ($\text{SiO}_2 + \text{Al}_2\text{O}_3 + \text{Fe}_2\text{O}_3 \geq 84\%$), with pozzolanicity at least as high as fly ash and similar to that of other masonry materials, such as masonry [4,23] and fired clay sanitary ware [24] rubble. Further to research on mechanical behaviour, GRC has no adverse effect on new eco-cement performance at low replacement ratios ($\leq 7\%$), whereas masonry ultrafines induce no significant decline in compressive or flexural strength at percentages of up to 25%.

Another line of research that has evoked considerable interest, as noted earlier, is the valorisation of agroforestry waste as an SCM. Two types of such waste are distinguished, depending on the origin [25]: laboratory-calcined ($500\text{ }^\circ\text{C} \leq T \leq 700\text{ }^\circ\text{C}$) biomass agroforestry waste (primarily bagasse, rice husk and to a lesser extent bamboo ash) [26–28]; and biomass or bottom ash, BA, from power and/or heat plants [29–32], which generate around 10 Mt of BA yearly [33]. SiO₂, Al₂O₃ and Fe₂O₃ ($\text{SiO}_2 + \text{Al}_2\text{O}_3 + \text{Fe}_2\text{O}_3 \geq 70\%$) are the majority compounds in such waste, which exhibits high early and late age lime fixation capacity (=pozzolanicity). No common pattern has been identified in the effect

of including such SCMs on end product mechanical performance, however, which has on the contrary been observed to depend on the origin and nature of the waste and the replacement ratio [30,34–36].

In that regard, no prior study has been published in the international literature assessing the durability of ternary or quaternary eco-cements, simultaneously bearing mixed C&DW ultrafines ($U_{C\&DW}$) and BA or both with silica fume ($U_{C\&DW} + BA + SF$).

The research described hereunder used the Koch and Steinegger method [37] to analyse the seawater-, chloride- and sulphate-resistance of cement pastes bearing 30% or 45% SCMs ($U_{C\&DW} + BA$ or $U_{C\&DW} + BA + SF$). Secondly, the processes governing cement decay were determined on the grounds of XRD-identified mineralogical variations and the morphological changes observed in the exposed materials with scanning electron microscopy. The variations in pore size distribution detected with mercury porosimetry were also explored.

2. Materials and Methods

For ready and more convenient reference, the materials and methods deployed in this study are described schematically below.

2.1. Materials

Waste material: biomass ultrafines (BA)

Supplier: Spanish power plant

Origin: herbaceous + woody (eucalyptus, fruit, pine tree, etc.)

Chemical composition: (Table 1) CaO + MgO + SiO₂ ~70 wt%; alkali content ~12 wt%; Al₂O₃ + Fe₂O₃ content ~7 wt%

Table 1. SCM chemical composition.

| Composition (wt%) | $U_{C\&DW}$ | BA | SF |
|--------------------------------|-------------|-------|-------|
| SiO ₂ | 50.10 | 52.75 | 97.94 |
| Al ₂ O ₃ | 11.82 | 3.19 | - |
| Fe ₂ O ₃ | 4.06 | 3.72 | 0.10 |
| MgO | 2.12 | 1.93 | 0.30 |
| CaO | 13.21 | 14.91 | 0.23 |
| Na ₂ O | 1.41 | 1.85 | 0.21 |
| SO ₃ | 0.76 | 2.26 | - |
| K ₂ O | 3.58 | 10.13 | 0.50 |
| P ₂ O ₅ | 0.19 | 1.64 | - |
| Cl- | 0.04 | 1.00 | 0.04 |
| Other oxides | 0.72 | 0.52 | 0.01 |
| LOI | 12.00 | 6.10 | 0.67 |

Note— $U_{C\&DW}$: mixed ultrafines; BA: bottom ash ultrafines; SF: silica fume.

XRD-determined mineralogical composition: amorphous hump at $2\theta = 20^\circ$ – 35° indicative of amorphous silica; diffraction lines characteristic of cristobalite and quartz; other crystalline phases: sylvite (KCl), calcite (CaCO₃), mullite (Al₆Si₂O₁₃), hematite (Fe₂O₃), and alkaline orthoclase-like alkaline feldspars (KAlSiO₃); all reported earlier as components in similar biomass waste [32].

Specific surface: 2800 cm²/g; density: 2.75 g/cm³.

Waste material: mixed C&DW ultrafines ($U_{C\&DW}$)

Origin: C&DW management plant in the Spanish province of Cáceres

Chemical composition: (Table 1) SiO₂ + Al₂O₃ + Fe₂O₃ ~66 wt%; CaO ~13 wt%; alkalis ~5 wt%; trace elements

Mineralogical composition (Figure 1): majority phases (as in other mixed C&DW recycled aggregates [38]) = quartz, feldspars (albite and orthoclase), phyllosilicates (chamosite and biotite) and hematite; traces of calcite.

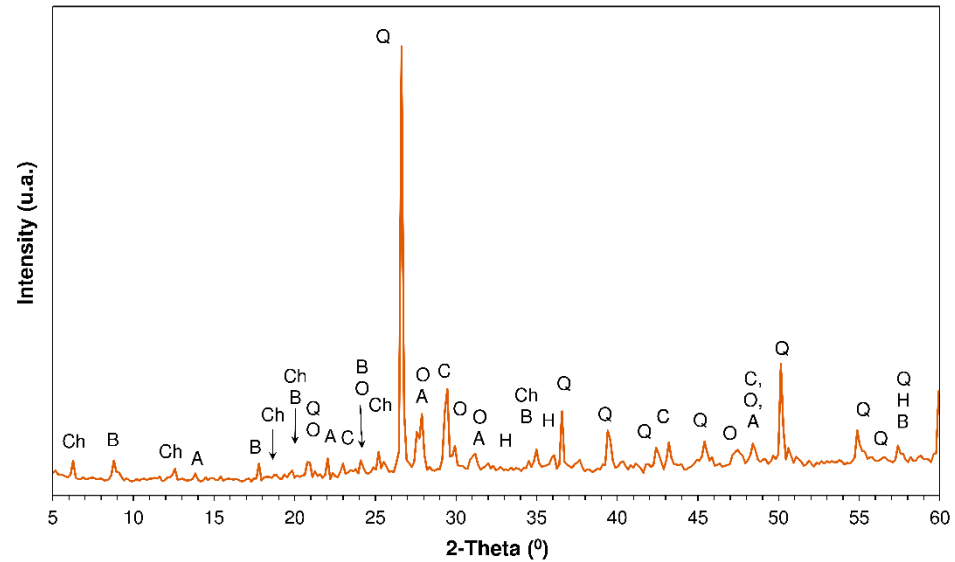


Figure 1. XRD pattern of the mixed construction and demolition waste ultrafine (Note—Chamosite; B: biotite; A: Albite; O: orthoclase; H: hematite; Q: quartz; and C: calcite).

Specific surface: 5700 cm²/g; density: 2.88 g/cm³.

Standardized supplementary cementitious materials: silica fume

Origin: commercial (Elkem Microwhite[®])

Characteristics: white; SiO₂ content ~98%, specific surface area ≥15 m²/g

Material: cement (OPC)

Class/strength: EN 197-1 [8]-compliant CEM I 42.5 R

Manufacturer: Lafarge plant, Villaluenga de la Sagra, Spanish province of Toledo

Specific surface: 3560 cm²/g; density: 3.1 g/cm³.

2.2. Blended Cements

M1

Components: 70%OPC + 20%U_{C&DW} + 10%BA, yielding a type II/B blended portland cement (21 % to 35 % total additions) or a type IV/A pozzolanic cement (11 % to 35 % total additions) in different proportions in keeping with European standard EBA, at replacement ratios of 10 % to 20 % according to the classification set out in standard EN 197-1 [8]

Physical, mechanical characteristics: Table 2

Table 2. New cement physical and mechanical properties.

| Property | Blended Cement | | | EN 197-1 Requirement | |
|----------------------------|----------------|-------|-------|----------------------|---------------------|
| | OPC | M1 | M2 | Strength Class 42.5 | Strength Class 32.5 |
| Physical | | | | | |
| Standard consistency (mm) | 32 | 34 | 34 | 34 ± 2 | |
| Initial setting time (min) | 200 | 170 | 190 | ≥60 | ≥75 |
| Expansion (mm) | 0 | 0 | 1 | ≤10 | ≤10 |
| Mechanical | | | | | |
| Compressive strength (MPa) | 7 days | 53.64 | 40.66 | 28.97 | ≥16.00 |
| | 28 days | 62.77 | 47.32 | 41.10 | ≥42.50 |
| | | | | | ≥32.50 |

EN 197-1-compliant: yes, for 28 d 42.5 MPa and 32.5 MPa ordinary cements

M2

Components: 55%OPC + 20%U_{C&DW} + 20%BA + 5%SF, yielding a type IV/B pozzolanic cement (36% to 55% total additions) in different proportions in keeping with European standards, at replacement ratios of 10% to 20% according to the classification set out in standard EN 197-1 [8]

Physical, mechanical characteristics: Table 2

EN 197-1-compliant: yes, for 28 d 32.5 MPa ordinary cements

2.3. Method

Paste preparation (OPC, M1, M2)

Water: deionised, w/c ratio = 0.5

Specimen number, shape, dimensions; 12 per blend, medium (seawater; chloride, sulphate solutions) and exposure time; prismatic; 1 × 1 × 6 cm

Moulding, curing: removal from moulds 24 h after casting, cured for 21 d at 100% RH and T = 20 ± 1 °C

Treatment

Soaking media: seawater (ASTM-D1141 [39]); 0.5 M sodium chloride, 0.3 M sodium sulphate; reference: deionised water (Koch–Steinegger method, [37,40]), deemed optimal for assessing blended cement resistance to such agents as it simultaneously accommodates the pozzolanic reaction and the assessment of its most prominent advantages [41]

Soaking time; T: 21 d, 56 d or 90 d; 20 °C

Procedure: specimens triple-washed in deionized water to remove any excess salt and dried in a laboratory kiln at 40 °C to a constant weight prior to characterisation at each exposure time

Mechanical and microstructural analysis

Parameters measured: flexural strength, chemical resistance and XRD-identification of new compounds at each age

Determination of chemical resistance to aggressive media: Koch–Steinegger corrosion index, calculated as (Equation (1)):

$$CI = \frac{F_{SX}}{F_{SW}} \quad (1)$$

where *CI* = corrosion index; *F_{SX}* = flexural strength at exposure time 'i' to medium 'X'; (*sw*: seawater; *chl*: 0.3 M NaCl; *s*: 0.5 M Na₂SO₄); *F_{SW}* = flexural strength in water-soaked specimens, same exposure times

Pore size distribution, SEM/EDX: in 56-d specimens

2.4. Instrumental Techniques

XRD (mineralogy)

Instrument: Bruker AXS D8 X-ray powder diffractometer

Specifications: 3-kW (Cu Ka1.2) copper anode; wolfram cathode X-ray generator

Scanning characteristics: 2θ angles of 5° to 60°; scanning rate, 2°/min

Voltage generator tube settings: 40 kV, 30 mA

SEM (microstructural analysis)

Instrument: Hitachi S4800 electron microscope

Specifications: coupled to a Bruker Nano XFlash 5030 silicon drift detector for EDX determination of chemical composition

MIP (porosity)

Instrument: Micromeritics Autopore IV 9500 mercury porosimeter

Specifications: measuring range, 0.006 μm to 175 μm; operating pressure: ≤33 000 psi (227.5 MPa) [42]

Mean pore size calculation (Equation (2)):

$$\varnothing_{med} = \frac{4 \cdot V}{A} \quad (2)$$

where *V* = median pore diameter (volume); *A* = median pore diameter (area)

Test frame (mechanical strength)

Instrument: IBERTEST AUTOTEST 200/10-SW test frame fitted with an adapter for $1 \times 1 \times 6$ cm specimens.

3. Results

3.1. Mechanical Properties

The decline in flexural strength values of the water-soaked cement and the materials exposed to seawater, sodium chloride (0.5 M NaCl) or sodium sulphate (0.3 M Na₂SO₄), was an indication that the effect of the dilution resulting from the lower amount of clinker present in new blends M1 and M2 was greater than the effect of the pozzolanicity of this type of SCMs (U_{C&DW} and BA). That finding was consistent with results reported by other authors who recorded declines in strength associated with smaller proportions of C-S-H gel and greater porosity in pastes prepared with SCMs processed from industrial by-products [36,43,44].

On the whole, strength rose with exposure time in the pastes exposed to seawater and 0.3 M Na₂SO₄. That pattern was associated with the formation of salts (see point 3.4) that would initially fill pores to generate a more compact matrix. Subsequent salt expansion, however, would raise inner stress and induce microcracking [41,45].

The rise in strength in the pastes exposed to 0.5 M NaCl may be attributed to: (i) the formation of more hydration product [46], favoured by the enhancement of Ca(OH)₂ solubility in NaCl solutions; (ii) greater C-S-H gel stability [47] with the uptake of some of the Na⁺ into the C-S-H interlayer spaces [48]; or (iii) Friedel's salt precipitation in the pores [49].

A comparison of the behaviour of the blends exposed to the three types of aggressive media is provided in Table 3. OPC and M1 were observed to follow a similar pattern except when soaked in seawater, where the simultaneous inclusion of the new SCMs (BA and U_{C&DW}) lowered strength by ~5 % relative to the water-soaked 90 d pastes. Of the pastes exposed to sodium chloride, performance declined the least in 90 d M1, to ~1 % below its water-soaked counterpart, compared to the ~9% decline observed for OPC. Strength rose in the same materials in the 90-d attack by Na₂SO₄, by 72% in OPC and 13% in M1.

Table 3. Flexural strength (MPa) of pastes soaked in water or aggressive media.

| Medium | Time (days) | Paste | | |
|---------------------------------------|-------------|---------------|--------------|--------------|
| | | OPC | M1 | M2 |
| Water | 21 | 10.04 ± 0.71 | 8.09 ± 0.85 | 8.87 ± 1.01 |
| | 56 | 9.39 ± 1.11 | 8.49 ± 0.93 | 8.33 ± 1.10 |
| | 90 | 10.59 ± 1.180 | 9.79 ± 1.04 | 9.09 ± 1.04 |
| Seawater | 21 | 11.29 ± 0.83 | 8.38 ± 0.26 | 8.12 ± 0.32 |
| | 56 | 12.79 ± 1.13 | 9.17 ± 0.37 | 6.51 ± 0.36 |
| | 90 | 13.14 ± 0.69 | 9.26 ± 0.61 | 5.57 ± 0.55 |
| 0.5 M NaCl | 21 | 9.84 ± 0.65 | 8.37 ± 0.67 | 8.16 ± 0.42 |
| | 56 | 9.73 ± 0.93 | 8.91 ± 0.63 | 8.44 ± 0.48 |
| | 90 | 9.68 ± 1.40 | 9.72 ± 0.58 | 8.36 ± 0.57 |
| 0.3 M Na ₂ SO ₄ | 21 | 14.41 ± 1.43 | 11.82 ± 0.98 | 10.00 ± 0.71 |
| | 56 | 17.24 ± 1.73 | 10.59 ± 1.21 | 9.12 ± 0.72 |
| | 90 | 18.24 ± 0.50 | 11.09 ± 1.03 | 8.91 ± 0.54 |

Note—OPC: ordinary portland cement; M1: 70%OPC + 20%U_{C&DW} + 10%BA; M2: 45%OPC + 20%U_{C&DW} + 20%BA + 5%SF.

The M2 blends (OPC + U_{C&DW} + BA + SF) exhibited lower performance than the other two pastes irrespective of the exposure medium. In the samples exposed to seawater, the

90 d values for M2 were ~38% lower than for OPC ~8% lower where the medium was 0.5 M NaCl and ~2% lower when attacked by 0.3 M Na₂SO₄. Those findings infer that including SF with the Ba + U_{C&DW} combination had no beneficial effect, possibly because the amount of portlandite present in the binder/SCM system was insufficient to support the pozzolanic reaction, which would be expected to generate a more compact and stronger matrix [50].

3.2. Porosity

Macro- and mesopore size distribution in the 56 d OPC, M1 and M2 pastes is graphed in Figure 2. The refinement in water-soaked paste M1 and M2 pore systems relative to OPC was attributable to the pozzolanic reaction between the SCMs and the portlandite generated during cement hydration. C-S-H gel, the predominant reaction product, would fill the pores, reducing the volume of macro- and raising the volume of mesopores [51].

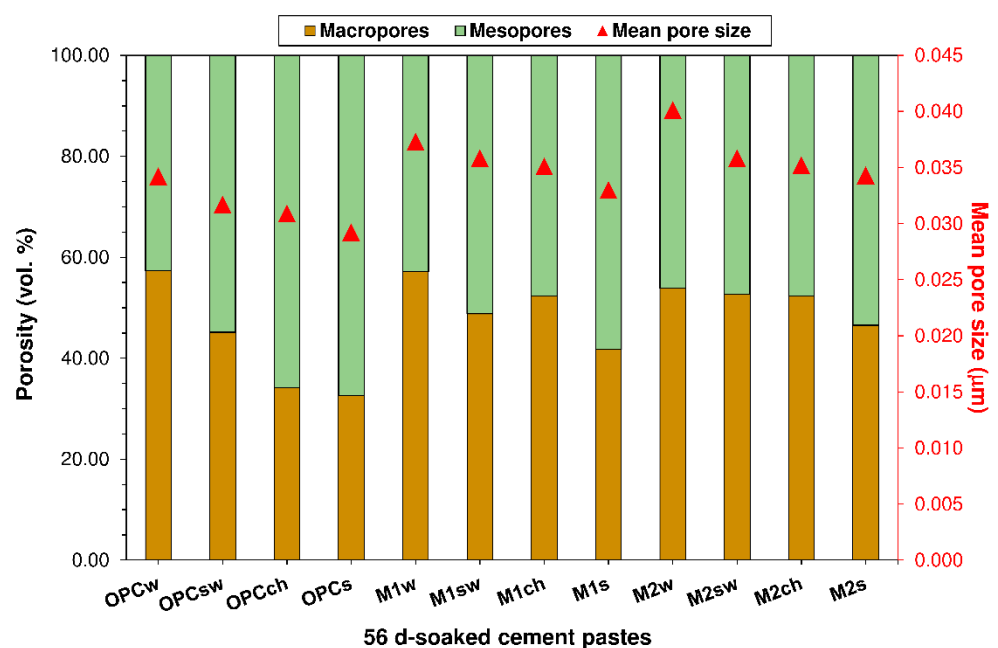


Figure 2. Pore systems in 56-d pastes exposed to distilled water (w), seawater (sw), 0.5 M NaCl (ch) or 0.3 M Na₂SO₄ (s).

The pore system in the OPC exposed to aggressive media was refined more intensely than the systems in pastes M1 or M2, enhancing its durability and inducing higher Kock & Steinegger indices (see Section 3.3). That finding is consistent with prior accelerated testing for durability in cement-based materials bearing fly ash and either silica/alumina nanoparticles [52] or masonry industry sludge [4].

The total porosity (Pt) values for the 56-d water- or aggressive medium-soaked pastes listed in Table 4 show that porosity was higher in SCM-bearing pastes M1 and M2 than in OPC due to the intrinsic effect of the blend of SCMs on that parameter. The decline in total porosity observed in the pastes exposed to the aggressive media relative to the water-soaked specimens was attributed to the precipitation of new products such as Friedel's salt, ettringite, gypsum and brucite resulting from the chemical attack on the pore system. Their presence induced a rise in mesopore volume [53–55] (Figure 2), lowering permeability and retarding decay [56]. The common denominator in all the pastes analysed was that the decline in Pt was steepest in 0.3 M Na₂SO₄ (followed by seawater and 0.5 M NaCl pastes in that order) and steeper than in the distilled water-soaked samples. That finding was closely associated with the nature of the products of the chemical attack [6].

Table 4. Total porosity (vol.%) in 56-d pastes.

| Medium | Paste | | |
|---------------------------------------|-------|-------|-------|
| | OPC | M1 | M2 |
| Water | 20.79 | 27.47 | 31.00 |
| Seawater | 19.14 | 27.19 | 30.31 |
| 0.5 M NaCl | 19.87 | 27.34 | 30.81 |
| 0.3 M Na ₂ SO ₄ | 17.99 | 25.47 | 28.59 |

Those patterns were consistent with prior reports of the behaviour of cement pastes bearing pozzolans such as blast furnace slag, fly ash, silica fume, C&DW or biomass waste after exposure to aggressive agents [20,25,56,57].

3.3. Corrosion Index

The OPC, M1 and M2 corrosion index/exposure time (t_{exp}) curves in Figure 3 show that in all the pastes, with the exception of seawater-soaked M2, an initial rise in the index ($t_{exp} \leq 56$ d) was followed by a decline after 90 d of exposure. Further to Koch–Steinegger criteria, pastes OPC, M1 and M2 could be deemed sulphate-resistant, for their 56-d corrosion index was greater than or equal to 0.70.

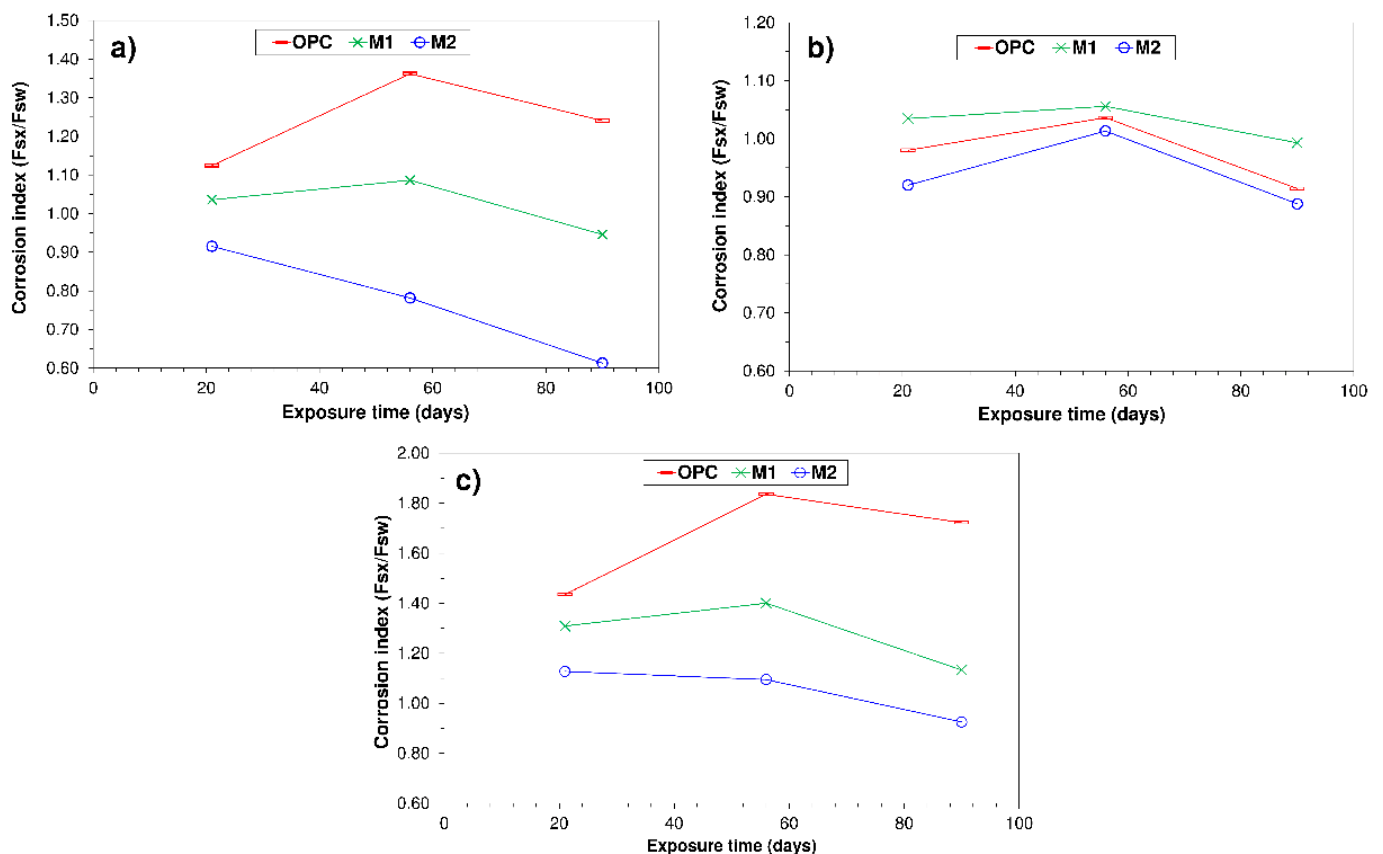


Figure 3. Corrosion indices over time in pastes OPC, M1 and M2 exposed to aggressive media: (a) seawater; (b) 0.5 M NaCl; (c) 0.3 M Na₂SO₄.

In this respect also, the inclusion of SF to the BA + U_{C&DW} blend was observed to have no beneficial effect on paste durability where the M1 corrosion index was consistently lower than the OPC value, irrespective of test age and aggressive medium.

3.4. X-ray Diffraction Findings

The XRD patterns for pastes OPC, M1 (70%OPC + 20%U_{C&DW} + 10%BA) and M2 (55%OPC + 20%U_{C&DW} + 20%BA + 5%SF) soaked in water or exposed to the aggressive media analysed are reproduced in Figures 4–7. The crystalline compounds identified in the water-soaked OPC specimens (Figure 3) included primarily calcium monocarboaluminate ($\text{CH}_{22}\text{Al}_2\text{Ca}_4\text{O}_{20}$), ettringite ($(\text{CaO})_6(\text{Al}_2\text{O}_3)(\text{SO}_3)_3 \cdot 32\text{H}_2\text{O}$), portlandite ($\text{Ca}(\text{OH})_2$), calcite (CaCO_3) and anhydrous dicalcium silicate (C_2S) in the form of larnite, a mineral present in portland cement detected by XRD after soaking in water because it hydrates more slowly than other mineralogical phases in the cement [58].

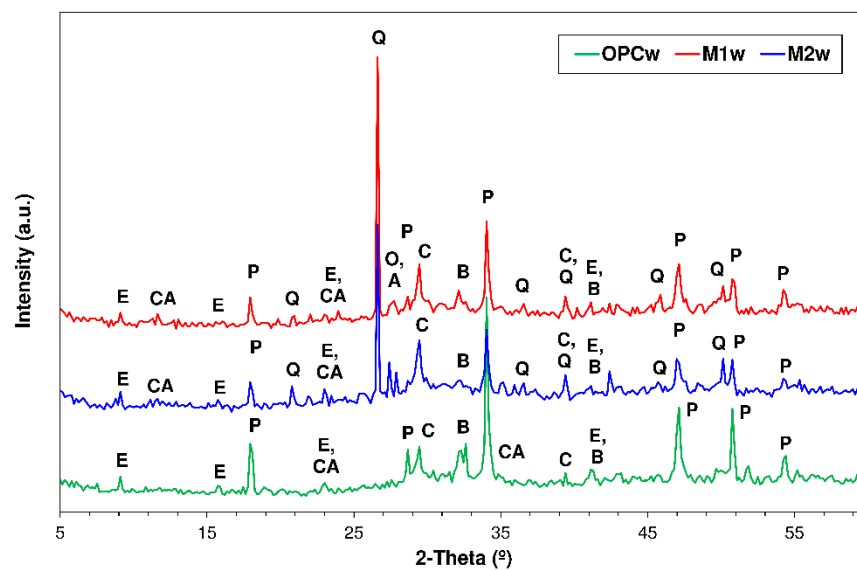


Figure 4. XRD patterns for 56-d-soaked pastes: OPC, M1 and M2 (Note—E: ettringite; CA: calcium monocarboaluminate; P: portlandite; Q: quartz; O: orthoclase; A: Albite; C: calcite; and B: belite).

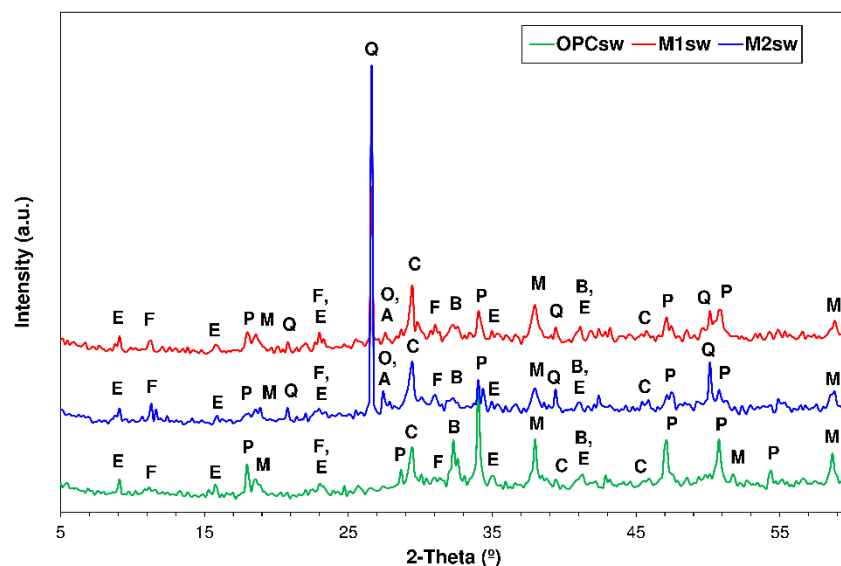


Figure 5. XRD patterns for 56 d OPC, M1 and M2 exposed to seawater (Note—E: ettringite; M: brucite; P: portlandite; Q: quartz; O: orthoclase; A: Albite; C: calcite; and B: belite).

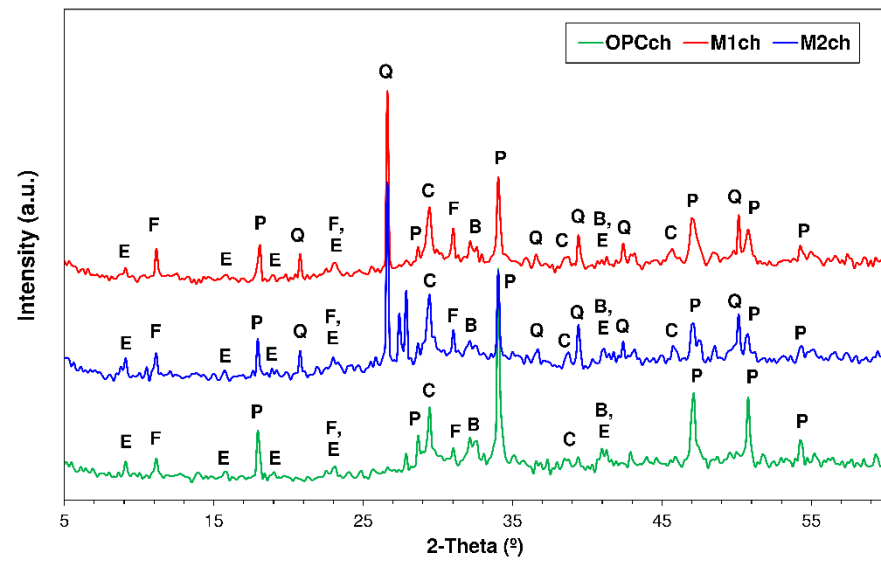


Figure 6. XRD patterns for 56-d OPC, M1 and M2 exposed to 0.5 M NaCl (Note—E: ettringite; F: Friedel's salt; P: portlandite; Q: quartz; O: orthoclase; A: Albite; C: calcite; and B: belite).

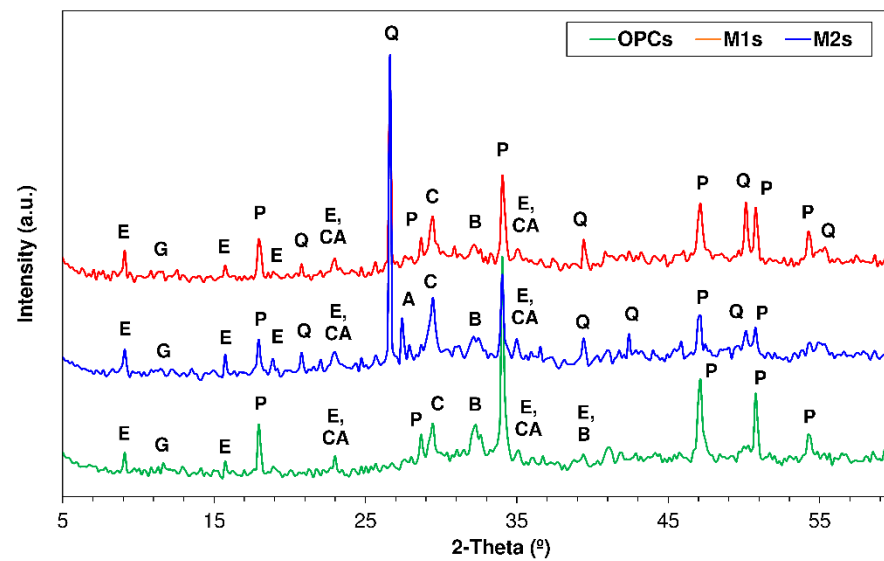


Figure 7. XRD patterns for 56 d OPC, M1 and M2 exposed to 0.3 M Na₂SO₄ (Note—E: ettringite; G: gypsum; CA: calcium monocarboaluminato; P: portlandite; Q: quartz; O: orthoclase; A: Albite; C: calcite; and B: belite).

The same phases as observed in OPC were identified in phases M1 and M2, along with quartz and the feldspars albite and orthoclase present in the SCMs used, as discussed in Section 2.1. The intensity of the portlandite reflections declined as a result not only of lower cement content, but also of the pozzolanic reaction induced by the U_{C&DW}, BA and SF added.

The calcium monocarboaluminato observed in the water-soaked specimens was absent in the pastes exposed to seawater (Figure 5). The diffractograms for the latter also contained lines for other crystalline compounds resulting from the reaction between hydration products and the sulphate and chloride ions in seawater. The Cl[−] ions diffusing through paste pores were partially retained by the phases bearing Al₂O₃, giving rise to calcium monochloraluminato hydrate or Friedel's salt (3CaO·Al₂O₃·CaCl₂·Al₂O₃·10H₂O) [59,60], from which ettringite may have formed via reaction with SO₄^{2−} ions [4]. Brucite (Mg(OH)₂) also formed as the product of the reaction between the Mg²⁺ in the seawater and the OH[−]

ions present in portlandite [61]. The brucite diffraction lines were more intense in the OPC than in M1 or M2 (see Section 3.4). The lines for portlandite were significantly less intense in the seawater- than in the water-soaked specimens, from which seawater may be inferred to have attacked that hydration product directly. In contrast, the ettringite and calcite lines were more intense due to the interaction between the phases in the paste and the sulphates and carbonates present in seawater, resulting in the formation of secondary ettringite [62] and calcite [61].

The pastes exposed to 0.5 M NaCl (Figure 6) were observed to form Friedel's salt as a product of the reaction between phases C_3A and C_4AF , thereby limiting the secondary formation of ettringite, an expansive mineral with a consequently adverse effect on cement-based materials. The intensity of the respective diffraction lines was greater in pastes M1 and M2 than in OPC. The intensity of the lines for ettringite remained unchanged relative to the water-soaked pastes, a finding consistent with Ekolu et al. [63] reports to the effect that ettringite remains stable at NaCl concentrations of 0.5 M or lower.

Specimen exposure to the action of Na_2SO_4 (Figure 7) translated primarily into a rise in the intensity of the diffraction line for ettringite. The gypsum ($Ca_2SO_4 \cdot 2H_2O$) formation identified with SEM/EDX (see Section 3.4), could not be corroborated via XRD because the respective diffraction line overlapped with the reflections for other phases present in the pastes, such as the monocarboaluminates ($2\theta = 11.7^\circ$) and quartz ($2\theta = 20.8^\circ$) [64].

3.5. SEM/EDX Microstructural Analysis

Micrographs of the C-S-H gels in water-soaked pastes are reproduced in Figure 8a–c. The EDX analysis (ten analyses/gel) showed that the Ca/Si ratio in the OPC gel was 2.0, compared to 1.7 in M1 and 1.9 in M2. The findings also showed that adding SCMs induced aluminium uptake in the gel, as reported earlier by other authors who used pozzolanic additions to partially replace clinker [22,24,36,57]. Inasmuch as the aluminium may have replaced Si in the gel structure, those findings would explain the lower Ca/Si ratio in the pastes bearing SCMs. Compact portlandite plates were observed in all the pastes analysed, although less frequently and in smaller mean sizes in paste M1 and M2 than in OPC, due to the pozzolanicity of the former. Those findings were consistent with the XRD data.

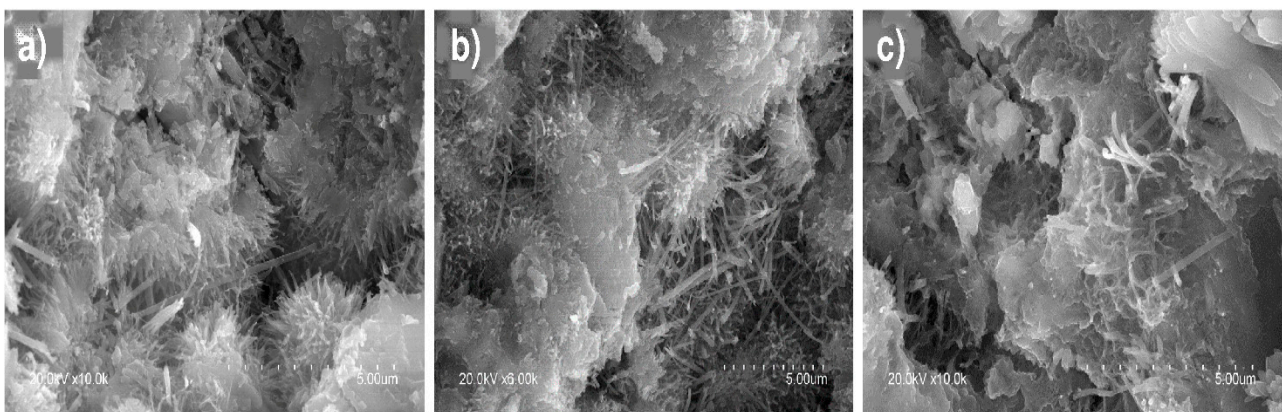


Figure 8. Calcium silicate hydrates (C-S-H gels) in 56-d water-soaked pastes: (a) OPC ($\times 6000$); (b) M1 ($\times 6000$); (c) M2 ($\times 10,000$).

Magnesium in the form of brucite predominated in the surface layer observed to form in all the 56-d pastes exposed to seawater (Figure 9a–c), corroborating the XRD findings. Brucite, the result of the reaction between portlandite and the $MgCl_2$ in seawater, was present on specimen surfaces only. The layer was thicker in the OPC ($e = 107.1 \mu m$) than in blend M1 ($e = 82.4 \mu m$) or M2 ($e = 83.5 \mu m$). Friedel's salt formation was also observed in seawater-soaked pastes OPC, M1 and M2, corroborating the XRD findings (Section 3.3).

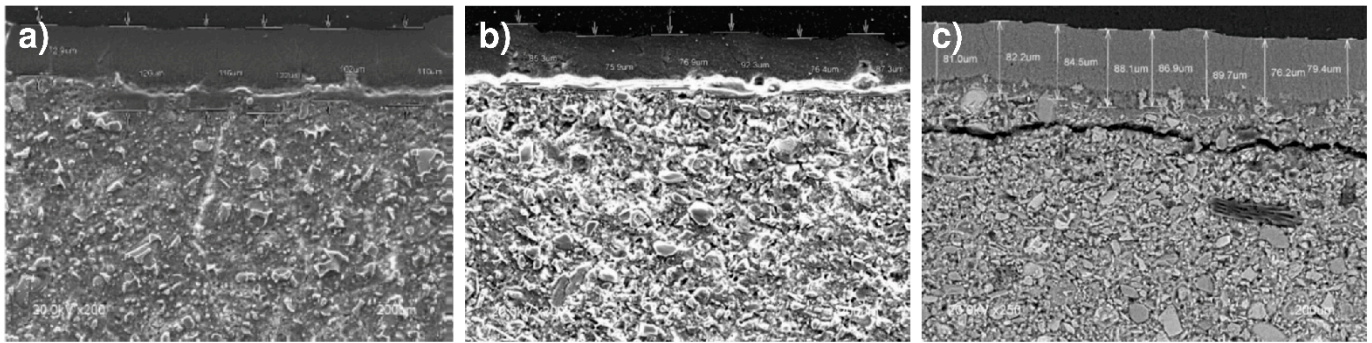


Figure 9. Brucite formation in 56-d seawater-soaked pastes: (a) OPC ($\times 200$); (b) M1 ($\times 200$); (c) M2 ($\times 250$).

Plates identified as Friedel's salt on the grounds of composition (Al, Cl and Ca) and morphology [60,65] were observed in the 56-d pastes exposed to 0.5 M NaCl (Figure 10).

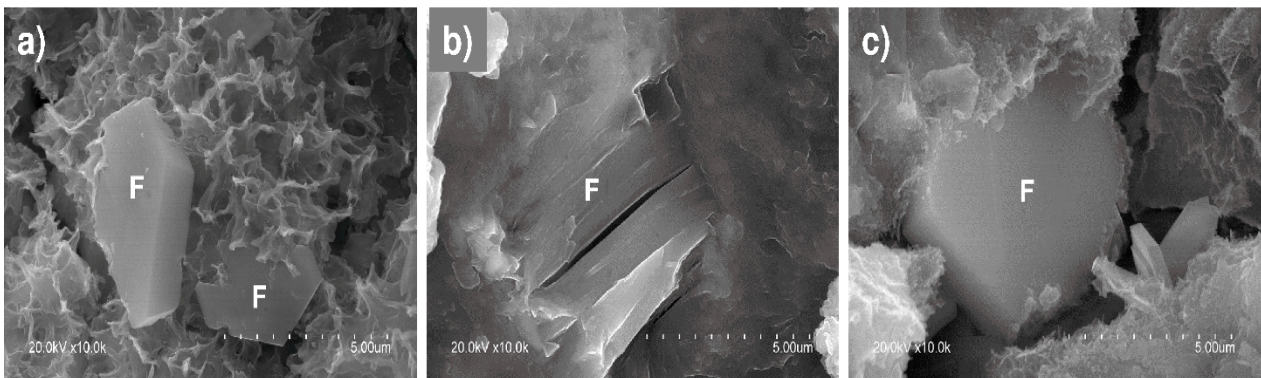


Figure 10. Friedel's salt in 56-d 0.5 M NaCl-soaked pastes ($\times 10,000$): (a) OPC; (b) M1; (c) M2.

The pastes exposed to the 0.3 M Na_2SO_4 solution were observed to form gypsum deposits clustering primarily in pores (Figure 11a), where the conditions for nucleation were most favourable [66,67]. Typically elongated needle-like ettringite (Figure 11b) was also identified [68,69], primarily inside pores [70], favoured by pressure conditions and the presence of the necessary ions [71,72]. For those very reasons, pores, together with cracks, are the sites where ettringite normally crystallises.

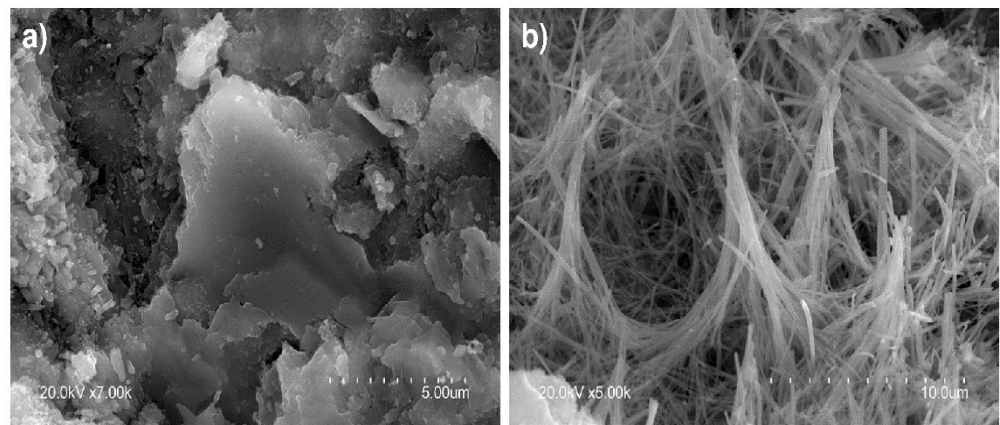


Figure 11. (a) Gypsum deposits ($\times 7000$) and (b) needle-like ettringite ($\times 5000$).

4. Conclusions

The following conclusions can be drawn from this study.

- Pastes bearing 30% (20% $U_{C\&DW}$ + 10%BA) SCMs exhibit 10% lower flexural strength than OPC and those with 45% (20% $U_{C\&DW}$ + 20%BA + 5%SF) supplementary cementitious materials 11% lower strength than the 56-d water-soaked pastes.
- As the pozzolanic reaction between SCMs and portlandite does not suffice to offset the dilution induced by a lower proportion of cement, the new pastes exhibit a larger mean pore size and greater porosity than OPC.
- Including $U_{C\&DW}$ + BA or $U_{C\&DW}$ + BA + SF yields cements able to resist the chemical attacks analysed, with a 56-d corrosion index >0.7 in all cases.
- Resistance to aggressive media attack is not enhanced by raising the percentage of SCM added, for the cements bearing the binary blend $U_{C\&DW}$ + BA proved to be more resistant than those to which silica fume was added.
- Paste M1 bearing 30% SCMs had a higher 56-d corrosion index, at 1.06, for the 0.5 M NaCl solution than both OPC (CI = 1.04) and M2 (CI = 1.02).
- OPC paste resists seawater and 0.3 M Na_2SO_4 better than M1, which in turn had a higher corrosion index than M2 irrespective of the medium.

The addition of $U_{C\&DW}$ + BA or $U_{C\&DW}$ + BA + SF prompts no significant change in cement paste morphology or in the compounds generated during the chemical attack.

Author Contributions: Conceptualisation, I.F.S.d.B., M.I.S.d.R., G.M., S.B., and C.M.; methodology, I.F.S.d.B., and G.M.; formal analysis, I.F.S.d.B., and G.M.; investigation, S.B., I.F.S.d.B., and G.M.; writing—original draft preparation, I.F.S.d.B., and G.M.; writing—review and editing, I.F.S.d.B., G.M., M.I.S.d.R., and C.M.; supervision, I.F.S.d.B., M.I.S.d.R. and C.M.; project administration, I.F.S.d.B. and G.M.; funding acquisition, M.I.S.d.R., and C.M. All authors have read and agreed to the published version of the manuscript.

Funding: This study was funded by the Spanish Ministry for Science and Innovation under project PID2019-107238RB-C21/AEI/10.13039/501100011033. It benefited as well from funding furnished by the Consejería de Economía, Ciencia y Agenda Digital from Junta de Extremadura under grant GR 18122 awarded to the MATERIA research group.

Institutional Review Board Statement: Not applicable.

Informed Consent Statement: Not applicable.

Data Availability Statement: Data sharing not applicable.

Acknowledgments: The cement supplied by the Lafarge Group plant Villaluenga de la Sagra, Toledo, Spain, is gratefully acknowledged.

Conflicts of Interest: The authors declare no conflict of interest.

References

1. Guo, H.; Dong, Y.; Gu, X. Durability assessment of reinforced concrete structures considering global warming: A performance-based engineering and experimental approach. *Constr. Build. Mater.* **2020**, *233*, 117251. [CrossRef]
2. Islam, R.; Nazifa, T.H.; Mohammed, S.F.; Zishan, M.A.; Yusof, Z.M.; Mong, S.G. Impacts of design deficiencies on maintenance cost of high-rise residential buildings and mitigation measures. *J. Build. Eng.* **2021**, *39*, 10221.
3. Yang, K.-H.; Lim, H.S.; Kwon, S.J.; Kim, J.H. Repair cost estimation techniques for reinforced concrete structures located at the seashore: Considering various probabilistic service life functions and actual mix proportions. *Constr. Build. Mater.* **2020**, *256*, 119469. [CrossRef]
4. Sánchez de Rojas, M.I.; Frías, M.; Sabador, E.; Asensio, E.; Rivera, J.; Medina, C. Durability and chromatic behavior in cement pastes containing ceramic industry milling and glazing by-products. *J. Am. Ceram. Soc.* **2019**, *102*, 1971–1981. [CrossRef]
5. Claisse, P.A. Cements and cement replacement materials. In *Civil Engineering Materials*; Butterworth-Heinemann: Oxford, UK, 2016; pp. 163–176.
6. Kumar Metha, P.; Monteiro, P.J.M. *Concrete: Microstructure, Properties and Materials*, 3rd ed.; McGraw-Hill: New York, NY, USA, 2006; p. 659.
7. UK Quality Ash Association. Fact Sheet 18—Embodied CO₂e of UK cement, additions and cementitious materials. Available online: https://cement.mineralproducts.org/documents/Factsheet_18.pdf (accessed on 15 June 2021).

8. European Committee for Standardization. *EN 197-1. Cement. Composition, Specifications and Conformity Criteria for Common Cements*; European Committee for Standardization: Geneva, Switzerland, 2011.
9. Villoria-Sáez, P.; Porras-Amores, C.; del Río Merino, M. Estimation of construction and demolition waste. In *Advances in Construction and Demolition Waste Recycling*; Woodhead Publishing: Sawston, UK, 2020; pp. 13–30.
10. Velardo, P.; Sáez del Bosque, I.F.; Matías, A.; Sánchez de Rojas, M.I.; Medina, C. Properties of concretes bearing mixed recycled aggregate with polymer-modified surfaces. *J. Build. Eng.* **2021**, *38*, 102211. [[CrossRef](#)]
11. Gonzalez-Fonteboa, B.; Seara-Paz, S.; de Brito, J.; Gonzalez-Taboada, I.; Martinez-Abella, F.; Vasco-Silva, R. Recycled concrete with coarse recycled aggregate. An overview and analysis. *Mater. Constr.* **2018**, *68*, e151. [[CrossRef](#)]
12. Plaza, P.; Sáez del Bosque, I.F.; Frías, M.; Sánchez de Rojas, M.I.; Medina, C. Use of recycled coarse and fine aggregates in structural eco-concretes. Physical and mechanical properties and CO₂ emissions. *Constr. Build. Mater.* **2021**, *285*, 122926. [[CrossRef](#)]
13. Moreno-Juez, J.; Vegas, I.J.; Gebremariam, A.T.; García-Cortés, V.; di Maio, F. Treatment of end-of-life concrete in an innovative heating-air classification system for circular cement-based products. *J. Clean Prod.* **2020**, *263*, 121515. [[CrossRef](#)]
14. Letelier, V.; Tarela, E.; Muñoz, P.; Moriconi, G. Combined effects of recycled hydrated cement and recycled aggregates on the mechanical properties of concrete. *Constr. Build. Mater.* **2017**, *132*, 365–375. [[CrossRef](#)]
15. Xiao, J.; Xiao, Y.; Liu, Y.; Ding, T. Carbon emission analyses of concretes made with recycled materials considering CO₂ uptake through carbonation absorption. *Struct. Concr.* **2021**, *22*, E58–E73. [[CrossRef](#)]
16. Sun, C.; Chen, L.; Xiao, J.; Singh, A.; Zeng, J. Compound utilization of construction and industrial waste as cementitious recycled powder in mortar. *Resour. Conserv. Recycl.* **2021**, *170*, 105561. [[CrossRef](#)]
17. Cantero, B.; Bravo, M.; de Brito, J.; Sáez del Bosque, I.F.; Medina, C. Assessment of the Permeability to Aggressive Agents of Concrete with Recycled Cement and Mixed Recycled Aggregate. *Appl. Sci.* **2021**, *11*, 3856. [[CrossRef](#)]
18. Caneda-Martínez, L.; Monasterio, M.; Moreno-Juez, J.; Martínez-Ramírez, S.; García, R.; Frías, M. Behaviour and Properties of Eco-Cement Pastes Elaborated with Recycled Concrete Powder from Construction and Demolition Wastes. *Materials* **2021**, *14*, 1299. [[CrossRef](#)] [[PubMed](#)]
19. Asensio, E.; Medina, C.; Frías, M.; Sánchez de Rojas, M.I. Use of clay-based construction and demolition waste as additions in the design of new low and very low heat of hydration cements. *Mater. Struct.* **2018**, *51*, 101. [[CrossRef](#)]
20. Asensio, E.; Medina, C.; Frías, M.; Sánchez de Rojas, M.I. Clay-based construction and demolition waste as a pozzolanic addition in blended cements. Effect on sulfate resistance. *Constr. Build. Mater.* **2016**, *127*, 950–958. [[CrossRef](#)]
21. Asensio, E.; Medina, C.; Frías, M.; Sánchez de Rojas, M.I. Characterization of Ceramic-Based Construction and Demolition Waste: Use as Pozzolan in Cements. *J. Am. Ceram. Soc.* **2016**, *99*, 4121–4127. [[CrossRef](#)]
22. Asensio, E.; Medina, C.; Frías, M.; Sánchez de Rojas, M.I. Fired clay-based construction and demolition waste as pozzolanic addition in cements. Design of new eco-efficient cements. *J. Clean Prod.* **2020**, *265*, 121610. [[CrossRef](#)]
23. Sánchez de Rojas, M.I.; Marin, F.; Rivera, J.; Frías, M. Morphology and properties in blended cements with ceramic wastes as a pozzolanic material. *J. Am. Ceram. Soc.* **2006**, *89*, 3701–3705. [[CrossRef](#)]
24. Medina, C.; Saez del Bosque, I.F.; Asensio, E.; Frías, M.; Sanchez de Rojas, M.I. Mineralogy and Microstructure of Hydrated Phases During the Pozzolanic Reaction in the Sanitary Ware Waste/Ca(OH)₂ System. *J. Am. Ceram. Soc.* **2016**, *99*, 340–348. [[CrossRef](#)]
25. Medina, J.M.; Sánchez de Rojas, M.I.; Sáez del Bosque, I.F.; Frías, M.; Medina, C. Sulfate Resistance in Cements Bearing Bottom Ash from Biomass-Fired Electric Power Plants. *Appl. Sci.* **2020**, *10*, 8982. [[CrossRef](#)]
26. Medina, C.; Sáez del Bosque, I.F.; Frías, M.; Sánchez de Rojas, M.I. Design and characterisation of ternary cements containing rice husk ash and fly ash. *Constr. Build. Mater.* **2018**, *187*, 65–76. [[CrossRef](#)]
27. Frías, M.; Savastano, H.; Villar, E.; Sánchez de Rojas, M.I.; Santos, S. Characterization and properties of blended cement matrices containing activated bamboo leaf wastes. *Cem. Concr. Compos.* **2012**, *34*, 1019–1023. [[CrossRef](#)]
28. Gonzalez-Kunz, R.N.; Pineda, P.; Bras, A.; Morillas, L. SPlant biomass ashes in cement-based building materials. Feasibility as eco-efficient structural mortars and grouts. *Sust. Cities Soc.* **2017**, *31*, 151–172. [[CrossRef](#)]
29. Rajamma, R.; Senff, L.; Ribeiro, M.J.; Labrincha, J.A.; Ball, R.J.; Allen, G.C.; Ferreira, V.M. Biomass fly ash effect on fresh and hardened state properties of cement based materials. *Compos. Pt. B Eng.* **2015**, *77*, 1–9. [[CrossRef](#)]
30. Ohenoja, K.; Wigren, V.; Osterbacka, J.; Illikainen, M. Mechanically Treated Fly Ash from Fluidized Bed Combustion of Peat, Wood, and Wastes in Concrete. *Waste Biomass Valorization* **2020**, *11*, 3071–3079. [[CrossRef](#)]
31. Sáez del Bosque, I.F.; Sánchez de Rojas, M.I.; Asensio, E.; Frías, M.; Medina, C. Industrial waste from biomass-fired electric power plants as alternative pozzolanic materials. In *Waste and By-Products in Cement-Based Materials*; Woodhead Publishing: Sawston, UK, 2021; pp. 243–282.
32. Medina, J.M.; Sáez del Bosque, I.F.; Frías, M.; Sánchez de Rojas, M.I.; Medina, C. Characterisation and valorisation of biomass waste as a possible addition in eco-cement design. *Mater. Struct.* **2017**, *50*, 207. [[CrossRef](#)]
33. Carevic, I.; Baricevic, A.; Stirmer, N.; Bajto, J.S. Correlation between physical and chemical properties of wood biomass ash and cement composites performances. *Constr. Build. Mater.* **2020**, *256*, 119450. [[CrossRef](#)]
34. Medina, J.M.; Sáez del Bosque, I.F.; Frías, M.; Sánchez de Rojas, M.I.; Medina, C. Design and properties of eco-friendly binary mortars containing ash from biomass-fuelled power plants. *Cem. Concr. Compos.* **2019**, *104*, 103372. [[CrossRef](#)]
35. Agrela, F.; Cabrera, M.; Morales, M.M.; Zamorano, M.; Alshaaer, M. Biomass fly ash and biomass bottom ash. In *New Trends in Eco-Efficient and Recycled Concrete*; Woodhead Publishing: Sawston, UK, 2019; pp. 23–58.

36. Sáez del Bosque, I.F.; Medina, J.M.; Frías, M.; Sánchez de Rojas, M.I.; Medina, C. Use of biomass-fired power plant bottom ash as an addition in new blended cements: Effect on the structure of the C-S-H gel formed during hydration. *Constr. Build. Mater.* **2019**, *228*, 117081. [[CrossRef](#)]
37. Koch, A.; Steinegger, U. A rapid test for cements for their behaviour under sulphate attack. *Zem-Kalk-Gips* **1960**, *7*, 317–324.
38. Cantero, B.; Sáez del Bosque, I.F.; Matías, A.; Sánchez de Rojas, M.I.; Medina, C. Effect of Recycled Aggregate on Performance of Granular Skeleton. *ACI Mater. J.* **2020**, *117*, 113–124. [[CrossRef](#)]
39. American Society for Testing and Material. *ASTM D1141. Standard Practice for the Preparation of Substitute Ocean Water*; ASTM: West Conshohocken, PA, USA, 2013.
40. Medina, G.; Sáez del Bosque, I.F.; Frias, M.; Sánchez de Rojas, M.I.; Medina, C. Sulfate Resistance in Cements Bearing Ornamental Granite Industry Sludge. *Materials* **2020**, *13*, 4081. [[CrossRef](#)]
41. Irassar, E.F. Sulfate resistance of blended cement: Prediction and relation with flexural strength. *Cem. Concr. Res.* **1990**, *20*, 209–218. [[CrossRef](#)]
42. American Society for Testing and Material. *D 4404-84: Test Method for Determination of Pore Volume and Pore Volume Distribution of Soil and Rock by Mercury Intrusion Porosimetry*; ASTM: West Conshohocken, PA, USA, 2004.
43. Medina, G.; Sáez del Bosque, I.F.; Frías, M.; Sánchez de Rojas, M.I.; Medina, C. Effect of Granite Waste on Binary Cement Hydration and Paste Performance: Statistical Analysis. *ACI Mater. J.* **2019**, *116*, 63–72. [[CrossRef](#)]
44. Medina, G.; Sáez del Bosque, I.F.; Frías, M.; Sánchez de Rojas, M.I.; Medina, C. Mineralogical study of granite waste in a pozzolan/Ca(OH)₂ system: Influence of the activation process. *Appl. Clay Sci.* **2017**, *135*, 362–371. [[CrossRef](#)]
45. Scherer, G.W. Stress from crystallization of salt. *Cem. Concr. Res.* **2004**, *34*, 1613–1624. [[CrossRef](#)]
46. Li, G.; Zhang, A.; Song, Z.; Liu, S.; Zhang, J. Ground granulated blast furnace slag effect on the durability of ternary cementitious system exposed to combined attack of chloride and sulfate. *Constr. Build. Mater.* **2018**, *158*, 640–648. [[CrossRef](#)]
47. Li, S.; Roy, D.M. Investigation of relations between porosity, pore structure, and C1—Diffusion of fly ash and blended cement pastes. *Cem. Concr. Res.* **1986**, *16*, 749–759. [[CrossRef](#)]
48. Florea, M.V.A.; Brouwers, H.J.H. Modelling of chloride binding related to hydration products in slag-blended cements. *Constr. Build. Mater.* **2014**, *64*, 421–430. [[CrossRef](#)]
49. Goni, S.; Frias, M.; Vigil de la Villa, R.; Garcia, R. Sodium chloride effect on durability of ternary blended cement. Microstructural characterization and strength. *Compos. Pt. B Eng.* **2013**, *54*, 163–168. [[CrossRef](#)]
50. Villar-Cociña, E.; Morales, E.V.; Santos, S.F.; Savastano, H.; Frías, M. Pozzolanic behavior of bamboo leaf ash: Characterization and determination of the kinetic parameters. *Cem. Concr. Compos.* **2011**, *33*, 68–73. [[CrossRef](#)]
51. McCarthy, M.J.; Dyer, T.D. Pozzolanas and Pozzolanic Materials. In *Lea's Chemistry of Cement and Concrete*, 5th ed.; Butterworth-Heinemann: Oxford, UK, 2019; pp. 363–467.
52. Bassuoni, M.T.; Rahman, M.M. Response of concrete to accelerated physical salt attack exposure. *Cem. Concr. Res.* **2016**, *79*, 395–408. [[CrossRef](#)]
53. Frias, M.; Goni, S.; Garcia, R.; Vigil, R. Seawater effect on durability of ternary cements. Synergy of chloride and sulphate ions. *Compos. Pt. B Eng.* **2013**, *46*, 173–178. [[CrossRef](#)]
54. Ikumi, T.; Cavalaro, S.H.P.; Segura, I. The role of porosity in external sulphate attack. *Cem. Concr. Compos.* **2019**, *97*, 1–12. [[CrossRef](#)]
55. Ikumi, T.; Segura, I. Numerical assessment of external sulfate attack in concrete structures. A review. *Cem. Concr. Res.* **2019**, *121*, 91–105. [[CrossRef](#)]
56. Liu, K.; Sun, D.; Wang, A.; Zhang, G.; Tang, J. Long-Term Performance of Blended Cement Paste Containing Fly Ash against Sodium Sulfate Attack. *J. Mater. Civ. Eng.* **2018**, *30*, 04018309. [[CrossRef](#)]
57. Taylor, H.F.W. *Cement Chemistry*, 2nd ed.; Thomas Telford Publishing: London, UK, 1997.
58. Richardson, I.G. The nature of the hydration products in hardened cement pastes. *Cem. Concr. Compos.* **2000**, *22*, 97–113. [[CrossRef](#)]
59. Saez del Bosque, I.F.; van den Heede, P.; de Belie, N.; Sanchez de Rojas, M.I.; Medina, C. Freeze-thaw resistance of concrete containing mixed aggregate and construction and demolition waste-added cement in water and de-icing salts. *Constr. Build. Mater.* **2020**, *259*, 119772. [[CrossRef](#)]
60. Friedel, P.M. Sur un chloro-aluminate de calcium hydraté se maclant par compression. *Bull. Soc. Franç. Minéral.* **1987**, *19*, 122–136.
61. De Weerd, K.; Lothenbach, B.; Geiker, M.R. Comparing chloride ingress from seawater and NaCl solution in Portland cement mortar. *Cem. Concr. Res.* **2019**, *115*, 80–89. [[CrossRef](#)]
62. Geng, J.; Easterbrook, D.; Li, L.; Mo, L. The stability of bound chlorides in cement paste with sulfate attack. *Cem. Concr. Res.* **2015**, *68*, 211–222. [[CrossRef](#)]
63. Ekolu, S.O.; Thomas, M.D.A.; Hooton, R.D. Pessimism effect of externally applied chlorides on expansion due to delayed ettringite formation: Proposed mechanism. *Cem. Concr. Res.* **2006**, *36*, 688–696. [[CrossRef](#)]
64. Caneda-Martínez, L.; Kunther, W.; Medina, C.; Sánchez de Rojas, M.I.; Frías, M. Exploring sulphate resistance of coal mining waste blended cements through experiments and thermodynamic modelling. *Cem. Concr. Compos.* **2021**, *121*, 104086. [[CrossRef](#)]
65. Birnin-Yauri, U.A.; Glasser, F.P. Friedel's salt, Ca₂Al(OH)₆(Cl,OH)·2H₂O: Its solid solutions and their role in chloride binding. *Cem. Concr. Res.* **1998**, *28*, 1713–1723. [[CrossRef](#)]

66. Santhanam, M.; Cohen, M.D.; Olek, J. Mechanism of sulfate attack: A fresh look: Part 2. Proposed mechanisms. *Cem. Concr. Res.* **2003**, *33*, 341–346. [[CrossRef](#)]
67. Xiong, C.; Jiang, L.; Xu, Y.; Song, Z.; Chu, H.; Guo, Q. Influences of exposure condition and sulfate salt type on deterioration of paste with and without fly ash. *Constr. Build. Mater.* **2016**, *113*, 951–963. [[CrossRef](#)]
68. Komatsu, R.; Mizukoshi, N.; Makida, K.; Tsukamoto, K. In-situ observation of ettringite crystals. *J. Cryst. Growth* **2009**, *311*, 1005–1008. [[CrossRef](#)]
69. Hewlett, P.C. *Lea's Chemistry of Cement and Concrete*, 4th ed.; Butterworth-Heinemann: Oxford, UK, 1998; p. 1053.
70. Neville, A.M. *Properties of Concrete*, 1st ed.; John Wiley & Sons: Hoboken, NJ, USA, 2008; p. 844.
71. Liu, Z.; Deng, D.; de Schutter, G. Does concrete suffer sulfate salt weathering? *Constr. Build. Mater.* **2014**, *66*, 692–701. [[CrossRef](#)]
72. Taylor, H.F.W.; Famy, C.; Scrivener, K.L. Delayed ettringite formation. *Cem. Concr. Res.* **2001**, *31*, 683–693. [[CrossRef](#)]